P-ISSN 1991-8941
E-ISSN 2706-6703
Vol. 19, No. 2 (2025)

Journal of University of Anbar for Pure Science
(JUAPS)

journal homepage: juaps.uoanbar.edu.iq

Open Access

Original Paper

Synergistic effects of Fe_2O_3 and carbonization on the morphological and optical properties of lignin/PVA composite films

Firdous M. Mahmood[1*], **Mazin A. Alalousi**[2], **Abbas Hasan Faris**[3]

[1]Department of Physics , College of Science, University of Anbar, Ramadi, Iraq
[2]Nanomaterials Research Center, University of Anbar, Ramadi, Iraq
[3]Department of Chemical and Petrochemical Engineering, College of Engineering,University of Anbar, Ramadi, Iraq

ARTICLE INFO

Received: 18/03/2025
Accepted: 07/05/2025
Available online: 19/11/2025
December Issue
10.37652/juaps.2025.158128.1363

Cite @ JUAPS

Corresponding author
Firdous M. Mahmood
fir22s2001@uoanbar.edu.iq

ABSTRACT

This study examines the structural and optical characteristics of lignin/polyvinyl alcohol composite films, with a particular emphasis on the influence of Fe2O3 incorporation and carbonization under a nitrogen atmosphere. Field-emission scanning electron microscopy (FE-SEM) analysis demonstrated that variations in Fe_2O_3 concentration induce significant morphological changes, transitioning from nanorod formations to fibrous structures as the concentration increases. Both the structural stability and porosity of the films were enhanced by the carbonization process, leading to the integration of Fe2O3 nanoparticles into the carbonized films. Raman spectroscopy implied shifts in the graphitic (G-band) and disordered (Dbrand) carbon structures, reversing enhancing graphitization at higher Fe_2O_3 concentrations. Photoluminescence study identified the emission peaks at 605 nm, 750 nm, and 857 nm, in agreement with carbon dots, defect states, and extended sp^2-hybridized carbon networks, respectively. Integrating Fe_2O_3 to appear other peaks, which confirmed $\pi - \pi^*$ transitions and Fe3+-related defects. These results underscore the key role of Fe_2O_3 and carbonization in modulating the Lignin/PVA: Fe2O3 films' properties, rendering it suitable for advanced sensors, supercapacitors, and catalysis applications. carbonization in modulating the material's properties, rendering it appropriate for advanced applications in sensors, supercapacitors, and catalysis.

Keywords: *Electrospinning, Lignin, Photoluminescence, Raman shift*

1 INTRODUCTION

Carbon nanomaterials (CNMs) have been of special interest due to their unique physicochemical properties, including mechanical stability, tunable electronic behavior, and optical tunability, along with intrinsic biocompatibility and overall chemical versatility. These properties render CNMs highly beneficial for diverse purposes, especially in sensing technologies. At the same time, biomass has proven to be a viable precursor of carbon material synthesis due to its high carbon content, affordability, and eco-friendliness. Carbon materials from biomass exhibit an environmentally friendly and scalable option compared to traditional production processes, under green chemistry principles [1–5]. There are various allotropic forms of CNMs, such as diamond, graphene, amorphous carbon, fullerenes, and carbon nanorods. They are classified based on their dimensionality: zero-dimensional (0-D), one-dimensional (1-D), and two-dimensional (2-D) forms [2].

Among these materials, carbon nanorods have been extensively studied due to their outstanding mechanical and electronic properties, making them suitable for applications, including supercapacitors, biosensors, and high-resolution imaging sensors [3]. The most popular techniques for manufacturing carbon nanorods, such

December 2025 issue – published 1 December 2025.

as carbon nanotubes, are chemical vapor deposition (CVD) and laser ablation. These techniques require high temperatures, complex, and expensive preparation conditions. This highlights the need for more sustainable and efficient manufacturing methods [4].

Carbon nanomaterials (CNMs) synthesized from biogas plant residual waste were characterized using advanced techniques, including Raman spectroscopy XRD. These materials demonstrated a specific capacitance of 371.88 $F.g^{-1}$, highlighting their potential for supercapacitor applications [6]. Y. Peng et al manufactured nitrogen-doped lignin-based carbon nanotubes via pyrolysis using modified lignin as raw materials. Multi-walled carbon nanotubes with diameters ranging from 10 to 80 nm enhance the selectivity for pyridine-N in L-NCNTs. They exhibit their compatibility with peaceful coexistence as non-toxic thermoresponsive agents in light-sensitizing drug delivery systems [7]. Abbas et al produced Graphene quantum dots GQDs with 0.5-4 nm and a thickness of 1-3 graphene layers using the green precursor of biomass waste. GQDs have been used as detectors for ferric ions (Fe^{3+}) [8]. Raman spectra and photoluminescence of CNMs are affected by the metal additions, such as Fe, Co, and Ni, associated with carbonization processes. This enhancement produces shifts in the D and G bands in Raman spectra, resulting in increased graphitization and reduced structural defects [9]. Additionally, carbonation processes have been shown to enhance the photoluminescence properties of carbon-based materials. That amelioration is reflected in increased electron mobility and structural stability within the carbon matrix [10]. Likewise, the interaction between mineral additions and carbonaceous materials during synthesis plays an essential role in modulating their functional properties, including electrical conductivity, surface area, and optical properties [8].

The incorporation of mineral additions and carbonation processes represents a promising approach to adjusting the properties of BioSource carbon materials, making them more acceptable for next-generation applications. This work scrutinizes the Raman and photoluminescence properties of lignin/PVA films and focuses on the impact of iron oxide (Fe_2O_3) on their structural and optical characteristics. To the best of the authors' knowledge, such inclusive analyses of the carbonized lignin/PVA systems, especially in the Fe_2O_3 incorporation, remain unexplored. This work aims to explain detailed insights into the interactions between lignin, PVA, and Fe_2O_3, as well as their collective impact on the Raman and PL behaviors of the resulting composite films.

2 MATERIALS AND METHODS

Lignin powder was chemically extracted from date palm tree waste. The awdust was dissolved in a 10% sodium hydroxide (NaOH) solution with a solid-to-solvent ratio of 1 : 10. The mixture was then subjected to a temperature of 150 °C for three hours to facilitate lignin extraction. Next, to remove insoluble residues, sulfuric acid (H_2SO_4) of 20% was gradually added to the filtered solution until the pH reached 2 . The final lignin powder was obtained by filtering and drying the precipitated lignin for a few days at 50°C. The spinning solution was prepared by dissolving Polyvinyl Alcohol (PVA) in DEMSO at 90°C for three hours with continuous stirring using a magnetic stirrer. Lignin was added to the PVA solution at 65°C with continuous stirring on a magnetic stirrer for 10 h . After the solution cooled, it was loaded into a 10 ml syringe supplied with a 21 -gauge needle. The solution was then electrospun at 16 kV between the needle and the rotating-cylinder collector onto N -type silicon wafers at a pumping rate of 0.6mlh^{-1}. The material was then placed in a tube furnace under a nitrogen atmosphere, with the temperature raised from 25°C to 300°C at 5°C/min, held for 5 minutes, and then increased to 700°C at 10 − 15°C/min for 3 h before being left to cool, as shown in Figure 1. The synthesized films were characterized using a field-emission electron microscope (FE-SEM), photoluminescence (PL), and Raman shift spectra.

3 RESULT AND DISCUSSION

3.1 FE-SEM analysis

FE-SEM results of the Lignin/PVA and Lignin/PVA: Fe_2O_3 films are shown in Figure 2. The morphology of the Lignin/PVA and Lignin/PVA: Fe_2O_3 films changed depending on the used concentrations of Fe_2O_3. The Lignin/PVA films consisted of bulk aggregates with an average size of 187 nm and smaller particles with a size of 26 nm. The addition of Fe_2O_3 at a concentration of 4 ppm produced nanorods with a diameter of 29 nm and a length of 112 nm . While increasing the concentration to 5 ppm led to a decrease in the density of the rods and a slight change in the diameter and an increase in the length to 130 nm. In contrast, increasing the concentration to 7 nm resulted in the disappearance of the rods and appearance of fibrous-like formations with a diameter of 45 nm and a length of 500 nm surrounded by particles of different

shapes with an average size of 56 nm .

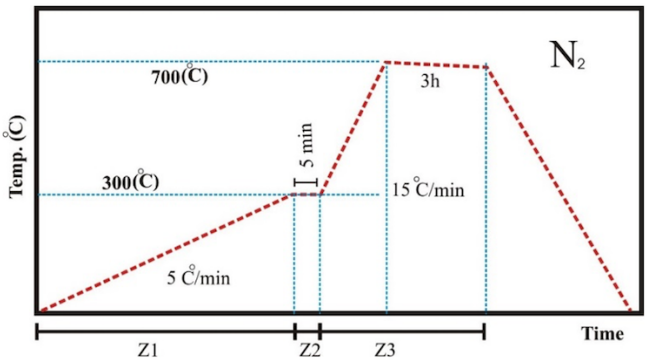

Fig. 1 Carbonization process

The carbonization in nitrogen also affected the morphological evolution of the composite films. Carbonization tends to break down organic materials such as PVA and lignin to form a carbon-rich matrix. The process can enhance the structural stability and porosity of the films as well as favor the embedding of Fe_2O_3 nanoparticles in the carbonized matrix. The synergistic effect of adding Fe_2O_3 and carbonization in a nitrogen atmosphere probably facilitated particle size redistribution and the observed morphological evolution, such as nanorod and fibrous structure formation.

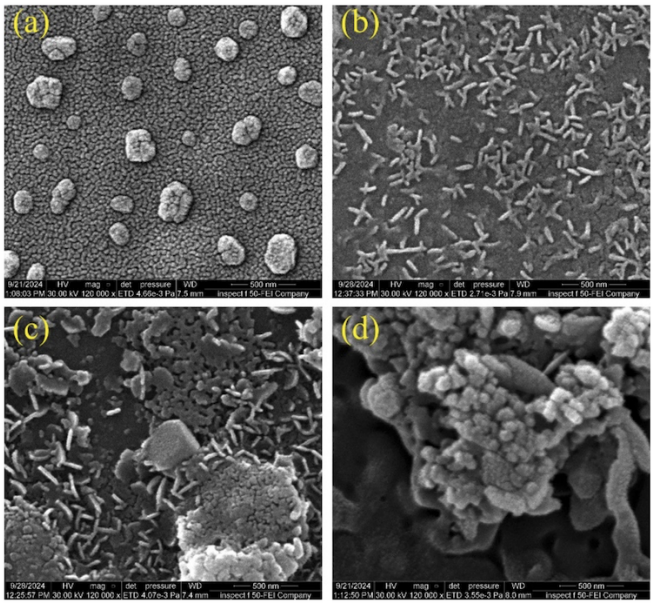

Fig. 2 FE-SEM images of (a) the Lignin/PVA and (b, c, and d) Lignin/PVA: Fe_2O_3 (4, 5, and 7) ppm films

3.2 Raman shift spectrum analysis

The Raman shift spectrum was used to analyze the carbonized lignin/PVA: Fe_2O_3 film (Figure 3). The peaks observed between 741 and 780 cm^{-1} are attributed to fluorescence resulting from the strong $C_\alpha = C_\beta$ bond [11]. However, the variations in these peaks with increasing Fe_2O_3 concentration suggest modifications in the lignin structure during carbonization, as well as chemical interactions between ferrite (Fe_2O_3) and the lignin/PVA matrix [12]. The peak appeared at 1625 cm^{-1}, corresponding to the G -band, is associated with C = C stretching vibrations in aromatic rings, which are characteristic of lignin [13]. A blue shift in this peak was observed when Fe_2O_3 was added at concentrations of 4 and 5 ppm, with shifts of 26 and 29 cm^{-1}, respectively, relative to the original vibration line at 1625 cm^{-1}. This shift emphasizes the influence of Fe_2O_3 on the interaction between lignin and PVA. These peaks are indicative of graphitic carbon (sp^2 hybridized carbon) and reflect the degree of graphitization [14]. Additionally, a distinct vibration peak at 1386 cm^{-1} emerged when the Fe_2O_3 concentration was increased to 7 ppm , which is associated with the D-band, representing disordered carbon structures [15]. The Raman spectrum analysis also indicated an unusual peak at 2025 cm^{-1} that could be attributed to C ≡ C stretching vibration in cumulenes or alkynes. The molecular structures may exist as impurities in carbonization. Although not that pronounced in comparison to the other peaks, this specific peak is highly informative about the subtle molecular changes involved in material preparation [16]. Furthermore, the peak at 2330 cm^{-1} is often associated with the presence of CO_2 or adsorbed CO_2 on the material's surface, which can occur during carbonization or due to environmental exposure. The 2836 cm^{-1} vibration line is typically described by C – H stretching vibrations of aliphatic hydrocarbons, such as methylene groups. The addition of Fe_2O_3 caused a red shift in the peak to 2809 cm^{-1}, indicating an increase in surface area that can potentially facilitate CO_2 interaction with the surface. This effect was especially pronounced at the 5 and 7 ppm concentrations of Fe 2 O 3 , where the peak shifted towards 2330 cm^{-1}, thereby increasing CO_2 adsorption [1]. Meanwhile, the band at 2836 cm^{-1} may be caused by symmetric stretching vibration of C – H bonds or other oxidative functional groups created during thermal treatment of carbonaceous material.

The occurrence of a peak at 3630 cm – 1 confirms the presence of O – H stretching vibrations, revealing

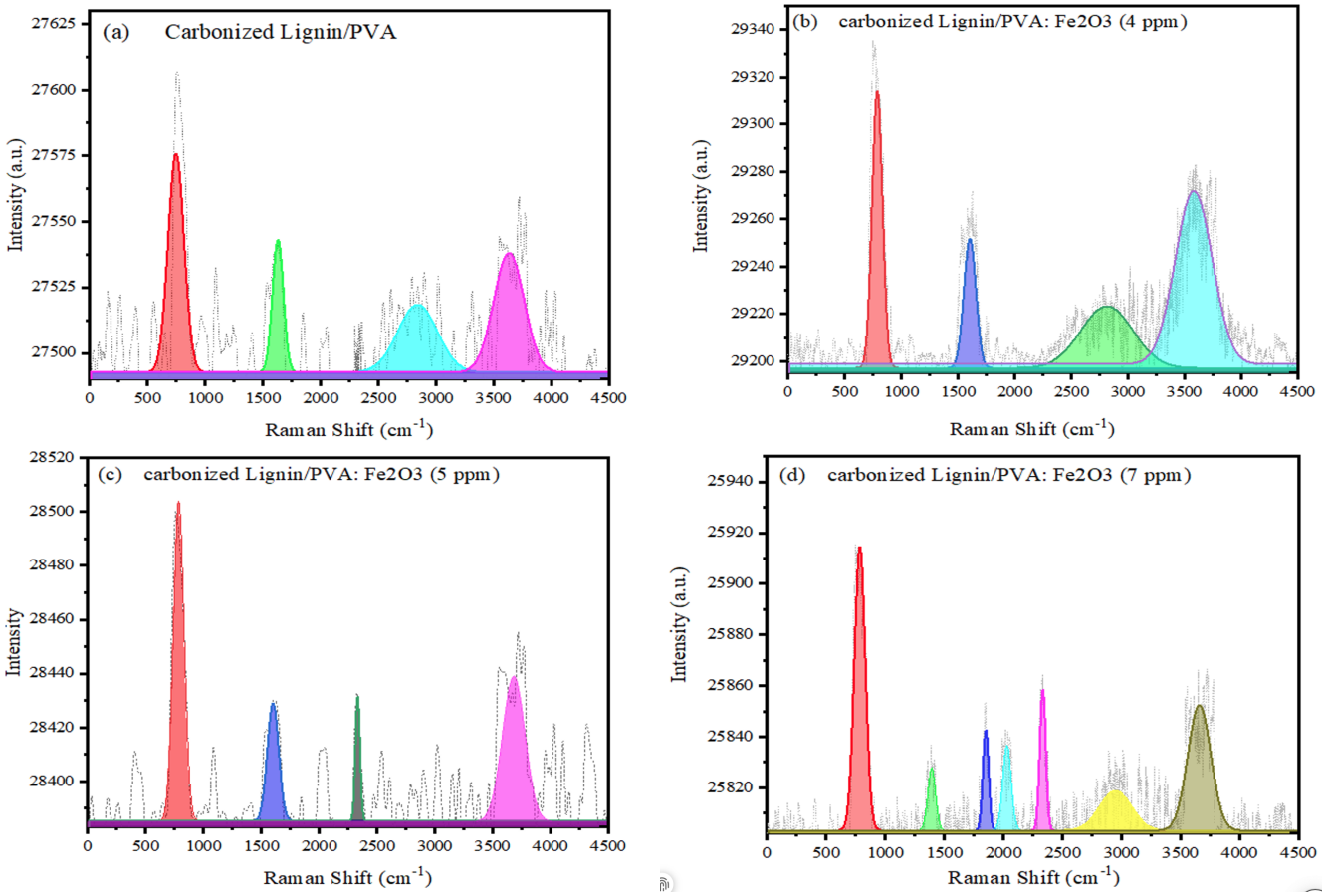

Fig. 3 Raman shift of (a) Lignin/PVA and (b, c, and d) Lignin/PVA: Fe_2O_3 (4, 5, and 7) ppm films

hydroxyl group bonding in lignin [17, 18]. Similarly, the peak at 2946 cm^{-1} confirms the presence of aliphatic CH_2 groups, which are common in lignin and PVA structures. The position and intensity of this peak indicate valuable information regarding the interactions between the organic materials (PVA and lignin) and inorganic Fe_2O_3 nanoparticles incorporated within the composite matrix. Peaks at 3630, 3582, 3682, and 3656 cm^{-1} are assigned to O – H stretching vibrations. These peaks are most probably caused by hydroxylated Fe_2O_3 (e.g., FeOOH), unreacted hydroxyl groups in lignin/PVA, or surface hydroxyls of the carbonized product. Fe_2O_3 can influence these peaks through increasing hydroxylation, modifying hydrogen bonding, or catalyzing the decomposition of organic -OH groups [19]. A higher Fe_2O_3 concentration of 7 ppm may enhance graphitization, leading to a more pronounced G -band and reduced defect density. In contrast, lower Fe_2O_3 concentrations (4 and 5 ppm) may result in less graphitization and higher defect density, consistent with the formation of nanorods and agglomerates, as observed in FE-SEM images [14, 20, 21]. The photoluminescence of lignin/polyvinyl alcohol (PVA) composites, as well as those mixed with iron oxide, was studied after carbonization by excitation with a 320 nm laser. Figure 4-a illustrates the emission spectrum with 605 nm , 750 nm , and 857 nm peaks for the carbonized lignin/ PVA, with the dominate 605 nm peak, which can be attributed to the $Hu \rightarrow T_1u$ transition [22]. The appearance and dominance of the 605 nm peak can be attributed to the possibility of carbon dots, the appearance of quantum effects, structural defects, and surface functional groups (e.g., -OH, -COOH), which create energy levels within the energy gap that facilitate radiative recombination processes [23].

The peak at 750 nm is usually assigned to emission from either defect states or energy levels induced by carbonization of lignin due to exciton recombination (electron-hole bound states). In the case of lignin-derived

carbon nanomaterials, this feature in the spectrum is characteristic of localized states that enable radiative recombination and thus fluorescence [24, 25]. The 857 nm emission occurs in the near-infrared (NIR) range, representing a longer wavelength and, by implication, lower energy transitions. This maximum is usually ascribed to larger conjugated systems like extended sp^2-hybridized carbon frameworks or polycyclic aromatic hydrocarbons, which experience lower energy emissions as a result of their electronic structure. The emission at longer wavelengths can also be explained by the "rededge effect," a phenomenon characterized by the emission spectrum's shift toward longer wavelengths as a result of the interactions occurring between emitting species and the environment. This is commonly seen in complex systems where environmental effects modulate the electronic transitions of the material [23].

When iron oxide was added at several concentrations (4,5 , and 7 ppm), peaks appeared at 439 nm and 451 nm , as shown in Figure 4 b – d.

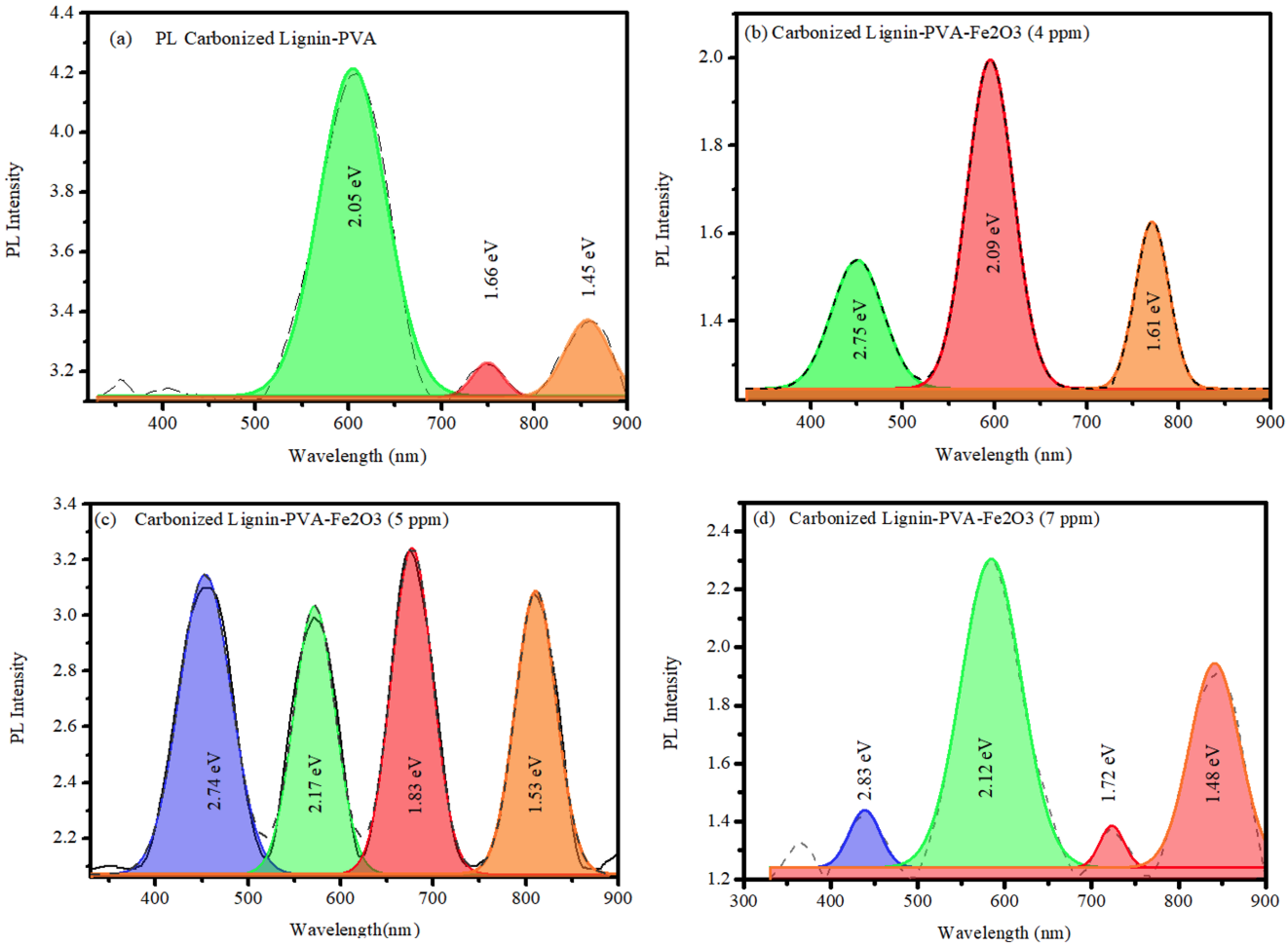

Fig. 4 Photoluminescence spectra of (a) the Lignin/PVA and (b, c, and d) Lignin/PVA: Fe_2O_3 (4, 5, and 7) ppm films

The 541 nm peak indicates the $\pi - \pi^*$ transition in the carbonized Lignin/PVA matrix [26] while the 595 nm peak indicates emission associated with defects such as oxygen vacancies or Fe^3-bound states [27]. The 771 nm peak also confirms the presence of deep defects and charge transitions involving iron ions. increase in the F_2O_3 concentrations to 5 and 7 ppm led to the blueshift and the redshifts suggest a change in the electronic structure of the carbonized matrix, possibly due to increased cross-linking or

quantum confinement effects and indicating further modification of defect states, likely due to increased F_2O_3 aggregation or the formation of larger Fe-related clusters, respectively [28, 29]. This behavior led from the fact that the incorporation of iron oxide into the lattice not only affected the disorder but also affected the vacancy sites, Oxygen, and its distribution. There is also a decrease in the spectral emission intensity with an increase in the concentration of the activator, iron oxide [30]. Table1 lists the PL peaks values of the carbonized (Lignin/ PVA and Lignin/ PVA/ Fe_2O_3) films.

Table 1 PL peaks values of the carbonized (Lignin/ PVA and Lignin/PVA/Fe_2O_3 Fe (4, 5, and 7) ppm films

Peak no.		Carbonized Lignin /PVA	Fe2O3 (4 ppm)	Fe2O3 (5 ppm)	Fe2O3 (7 ppm)
1	Energy (eV)	2.05	2.75	2.75	2.82
	Wavelength (nm)	605	451	451	439
2	Energy (eV)	1.653	2.084	2.168	2.119
	Wavelength (nm)	750	595	572	585
3	Energy (eV)	1.447	1.608	1.831	1.712
	Wavelength (nm)	857	771	677	724
4	Energy (eV)	2.83	2.12	1.53	1.473
	Wavelength (nm)	438	585	810	842

4 CONCLUSION

Waste palm biomass can be used as an economic precursor for the production of carbon nanorods. It provides a green alternative to traditional carbon nanomaterial synthesis. Addition of iron oxide (Fe_2O_3) to lignin/PVA composite films, followed by controlled carbonization in a nitrogen atmosphere, has a significant influence on the morphology, structure, and optical properties of the material. Using Fe_2O_3 serves as a catalyst and structural modifier that promotes nanorod growth, enhances graphitization, and regulates defect density. Raman spectra and photoluminescence measurements revealed that Fe_2O_3 induces large vibrational band shifts and emission profiles, characteristic of electronic structure and defect state changes, that are dependent on concentration. The results reflect the potential of carbonized lignin/PVA: Fe_2O_3 composites as high-performance, multi-purpose sensing and optoelectronic device materials, demonstrating the synergistic benefits of biomass-derived carbon, polymer matrices, and transition metal oxides in the fabrication of scalable, green nanomaterials for innovative technologies.

ACKNOWLEDGEMENT

N/A

FUNDING SOURCE

No funds received.

DATA AVAILABILITY

N/A

DECLARATIONS

Conflict of interest

The authors declare that they have no known competing financial interests or personal relationships that could have appeared to influence the work reported in this paper.

Consent to publish

All authors consent to the publication of this work. Written informed consent for publication was obtained from the participants.

Ethical approval

N/A

REFERENCES

[1] Omoriyekomwan JE, Tahmasebi A, Zhang J, Yu J. Mechanistic study on direct synthesis of carbon nanotubes from cellulose by means of microwave pyrolysis. Energy Conversion and Management. 2019;192:88–99. 10.1016/j.enconman.2019.04.042

[2] Shirvanimoghaddam K, Czech B, Abolhasani MM, Naebe M. Sustainable periodically patterned carbon nanotube for environmental application: Introducing the cheetah skin structure. Journal of Cleaner Production. 2018;179:429–440. 10.1016/j.jclepro.2018.01.145

[3] Ganesan S, Kalimuthu R, Kanagaraj T, Kulandaivelu R, Nagappan R, Pragasan LA, et al.

Microwave-assisted green synthesis of multifunctional carbon quantum dots as efficient fluorescence sensor for ultra-trace level monitoring of ammonia in environmental water. Environmental Research. 2022;206:112589. 10.1016/j.envres.2021.112589

[4] Esohe Omoriyekomwan J, Tahmasebi A, Zhang J, Yu J. Synthesis of Super-Long Carbon Nanotubes from Cellulosic Biomass under Microwave Radiation. Nanomaterials. 2022;12(5):737. 10.3390/nano12050737

[5] Zhang W, Qiu X, Wang C, Zhong L, Fu F, Zhu J, et al. Lignin derived carbon materials: current status and future trends. Carbon Research. 2022;1(1). 10.1007/s44246-022-00009-1

[6] Pathak M, Moravkova Z, Tatrari G, Bhatt D, Wadhwa P, Dhali S, et al. Bulk scale synthesis of high-performance carbon nanomaterial from biogas plant residual waste: Tuned porosity and composition for advanced supercapacitor applications. Diamond and Related Materials. 2024;149:111542. 10.1016/j.diamond.2024.111542

[7] Peng Y, Guo B, Wang W, Yu P, Wu Z, Shao L, et al. Efficient preparation of nitrogen-doped lignin-based carbon nanotubes and the selectivity of nitrogen speciation for photothermal therapy. International Journal of Biological Macromolecules. 2023;238:124127. 10.1016/j.ijbiomac.2023.124127

[8] Abbas A, Rubab S, Rehman A, Irfan S, Sharif HMA, Liang Q, et al. One-step green synthesis of biomass-derived graphene quantum dots as a highly selective optical sensing probe. Materials Today Chemistry. 2023;30:101555. 10.1016/j.mtchem.2023.101555

[9] Baptista FR, Belhout SA, Giordani S, Quinn SJ. Recent developments in carbon nanomaterial sensors. Chemical Society Reviews. 2015;44(13):4433–4453. 10.1039/c4cs00379a

[10] Zhang P, Zheng Y, Ren L, Li S, Feng M, Zhang Q, et al. The Enhanced Photoluminescence Properties of Carbon Dots Derived from Glucose: The Effect of Natural Oxidation. Nanomaterials. 2024;14(11):970. 10.3390/nano14110970

[11] Barsberg S, Matousek P, Towrie M. Structural Analysis of Lignin by Resonance Raman Spectroscopy. Macromolecular Bioscience. 2005;5(8):743–752. 10.1002/mabi.200500042

[12] Gierlinger N, Keplinger T, Harrington M, Schwanninger M. In: Raman Imaging of Lignocellulosic Feedstock. InTech; 2013. 10.5772/50878

[13] Moosavinejad SM, Madhoushi M, Vakili M, Rasouli D. Evaluation of degradation in chemical compounds of wood in historical buildings using FT-IR and FT-Raman vibrational spectroscopy. Maderas Ciencia y tecnología. 2019;(ahead):0–0. 10.4067/s0718-221x2019005000310

[14] Sadezky A, Muckenhuber H, Grothe H, Niessner R, Pöschl U. Raman microspectroscopy of soot and related carbonaceous materials: Spectral analysis and structural information. Carbon. 2005;43(8):1731–1742. 10.1016/j.carbon.2005.02.018

[15] García-Mateos FJ, Berenguer R, Valero-Romero MJ, Rodríguez-Mirasol J, Cordero T. Phosphorus functionalization for the rapid preparation of highly nanoporous submicron-diameter carbon fibers by electrospinning of lignin solutions. Journal of Materials Chemistry A. 2018;6(3):1219–1233. 10.1039/c7ta08788h

[16] Ferrari AC, Robertson J. Interpretation of Raman spectra of disordered and amorphous carbon. Physical Review B. 2000;61(20):14095–14107. 10.1103/physrevb.61.14095

[17] Liu Y, Cao L, Wang L, Qi Y, Zhao Y, Lu H, et al. Preparation and Application of Degradable Lignin/Poly (Vinyl Alcohol) Polymers as Urea Slow-Release Coating Materials. Molecules. 2024;29(8):1699. 10.3390/molecules29081699

[18] Alves JF, Edwards HGM, Korsakov A, de Oliveira LFC. Revisiting the Raman Spectra of Carbonate Minerals. Minerals. 2023;13(11):1358. 10.3390/min13111358

[19] de Haro JC, Tatsi E, Fagiolari L, Bonomo M, Barolo C, Turri S, et al. Lignin-Based Polymer Electrolyte Membranes for Sustainable Aqueous Dye-Sensitized Solar Cells. ACS Sustainable Chemistry & Engineering. 2021;9(25):8550–8560. 10.1021/acssuschemeng.1c01882

[20] Zhao X, Zhang X, Gao C, Wang P, He Y, Chu D, et al. Mechanism of carbon nanotube growth by Fe catalysts in a one-step process. Applied Physics A. 2025;131(3). 10.1007/s00339-025-08319-y

[21] Zhao Y, Wang J, Huang H, Cong T, Yang S, Chen H, et al. Growth of Carbon Nanocoils by Porous α-Fe2O3/SnO2 Catalyst and Its Buckypaper for High Efficient Adsorption. Nano-Micro Letters. 2020;12(1). 10.1007/s40820-019-0365-y

[22] Saraswati TE, Setiawan UH, Ihsan MR, Isnaeni I, Herbani Y. The Study of the Optical Properties of C60 Fullerene in Different Organic Solvents. Open Chemistry. 2019;17(1):1198–1212. 10.1515/chem-2019-0117

[23] Zhu S, Zhang J, Tang S, Qiao C, Wang L, Wang H, et al. Surface Chemistry Routes to Modulate the Photoluminescence of Graphene Quantum Dots: From Fluorescence Mechanism to Up-Conversion Bioimaging Applications. Advanced Functional Materials. 2012;22(22):4732–4740. 10.1002/adfm.201201499

[24] Krasley AT, Li E, Galeana JM, Bulumulla C, Beyene AG, Demirer GS. Carbon Nanomaterial Fluorescent Probes and Their Biological Applications. Chemical Reviews. 2024;124(6):3085–3185. 10.1021/acs.chemrev.3c00581

[25] Cao X, Li X, Wu R, Liu B, Lin W. Enhancing the Performance of Biodegradable Lignin Nanoparticle/PVA Composite Films via Phenolation Pretreatment of Lignin Using a Novel Ternary Deep Eutectic Solvent. Coatings. 2024;14(12):1544. 10.3390/coatings14121544

[26] Peng Y, Zhang X, Sun R, Zhang X, Ge C, Liu Y. Review of electro-spun carbon nanofiber electrode materials for electrochemical capacitors. Journal of Materials Chemistry A. 2024;12(47):32566–32592. 10.1039/d4ta06221c

[27] Shen Y, Luo C, Chen C, Zhang X, Shi M, Gu Z, et al. High-Temperature Resistance Photoluminescence Carbonized Polymer Dots Through Equilibrium Bi-Confinement Effects. Advanced Materials. 2024;37(5). 10.1002/adma.202407811

[28] Lassoued A, Lassoued MS, Dkhil B, Ammar S, Gadri A. Synthesis, photoluminescence and Magnetic properties of iron oxide (α-Fe2O3) nanoparticles through precipitation or hydrothermal methods. Physica E: Low-dimensional Systems and Nanostructures. 2018;101:212–219. 10.1016/j.physe.2018.04.009

[29] Zotov N, Yanev Y, Piriou B. Time-resolved luminescence of Fe 3+ and Mn 2+ ions in hydrous volcanic glasses. Physics and Chemistry of Minerals. 2002;29(4):291–299. 10.1007/s00269-001-0233-3

[30] Kaur J, Shah J, Kotnala RK, Verma KC. Raman spectra, photoluminescence and ferromagnetism of pure, Co and Fe doped SnO2 nanoparticles. Ceramics International. 2012;38(7):5563–5570. 10.1016/j.ceramint.2012.03.075

How to cite this article

Mahmood FM, Alalousi MA, Faris AH. Synergistic effects of Fe_2O_3 and carbonization on the morphological and optical properties of lignin/PVA composite films. Journal of University of Anbar for Pure Science. 2025; 19(2):126-133. doi:10.37652/juaps.2025.158128.1363